coatings

MDPI

Article

Corrosion Behavior of Aluminum Alloys in Different Alkaline Environments: Effect of Alloying Elements and Anodization Treatments

Riccardo Fabris, Giulia Masi and Maria Chiara Bignozzi *

Department of Civil, Chemical, Environmental and Materials Engineering (DICAM), University of Bologna, Via Terracini 28, 40131 Bologna, Italy; riccardo.fabris2@unibo.it (R.F.); giulia.masi5@unibo.it (G.M.)
* Correspondence: maria.bignozzi@unibo.it

Abstract: Aluminum alloys are extensively used to manufacture mechanical components. However, when exposed to alkaline environments, like lubricants, refrigerants, or detergents, they can be corroded, reducing their durability. For this reason, the aim of this study is to investigate the influence of aggressive alkaline solutions (i.e., pH and presence of chlorides) on the corrosion resistance of three aluminum alloys (AA 5083-H111, AA 6082-T6, and AA 7075-T6) with and without anodizing treatments. Open circuit potential (E_{OCP}) and anodic polarization measurements were carried out and typical corrosion parameters such as corrosion current density (i_{cor}) and corrosion rate (CR) were determined. Morphology of the corrosion attack and samples microstructure were investigated by scanning electron microscope. Results show that corrosion behavior of the three investigated alloys is influenced by (i) the aggressiveness of the testing environments; (ii) the thickness of the anodizing treatment; (iii) the alloy chemical composition; (iv) the distribution of intermetallic phases in the aluminum matrix. Moreover, three galvanic series have been built also testing other metallic alloys commonly used in mechanical applications, i.e., carbon steel (C40), stainless-steel (AISI 304), and Cu-based alloys (Cu-Ni alloy and CW 617 N, respectively). Results clearly indicate that galvanic series play a fundamental role when it is necessary to select an alloy for a specific environment, highlighting the thermodynamic conditions for corrosion occurrence. On the other hand, kinetic measurements and microstructural studies carried out on the three aluminum alloys stress the importance of the surface treatments and relevant thickness as well as the effect of metal exposure. Future work will involve the study of other surface treatments on aluminum alloys and the evaluation of their corrosion behavior in acidic environments.

Keywords: aluminum alloys; alkaline environment; corrosion behavior; corrosion rate

check for updates

Citation: Fabris, R.; Masi, G.; Bignozzi, M.C. Corrosion Behavior of Aluminum Alloys in Different Alkaline Environments: Effect of Alloying Elements and Anodization Treatments. *Coatings* **2024**, *14*, 240. https://doi.org/10.3390/coatings14020240

Academic Editor: Chi Tat Kwok

Received: 31 December 2023
Revised: 11 February 2024
Accepted: 16 February 2024
Published: 19 February 2024

Copyright: © 2024 by the authors. Licensee MDPI, Basel, Switzerland. This article is an open access article distributed under the terms and conditions of the Creative Commons Attribution (CC BY) license (https://creativecommons.org/licenses/by/4.0/).

1. Introduction

Nowadays, in the field of the mechanical industry, the design strategy adopted to manufacture machinery aims at developing high-performing systems with high productivity. Additionally, industrial plant operations may involve different conditions such as overloads, high temperatures, and quick temperature variations. To deal with all these operating conditions, machinery is usually designed and made of different metallic materials characterized by various performances (e.g., high strength, toughness, lightness, hardness, corrosion resistance, etc.). In particular, the most common metallic alloys normally used are carbon steel, stainless steel, and aluminum- and copper-based alloys [1–3]. Aluminum alloys (AAs) are the lightest alloys (density of 2.7 g/cm^3) among all the above-mentioned. In addition, they have good mechanical properties, such as static and dynamic strength, good electrical and thermal conductivity, and good resistance to atmospheric corrosion, as well as good technological properties, such as machinability, weldability, and castability [4,5]. All these properties allow designers to adopt a lightweight design approach when

manufacturing mechanical parts with a high strength-to-weight ratio, thus reducing the global weight of the machinery [6–8].

However, high-performing technical fluids like lubricants, refrigerants, or detergents are often required to ensure correct industrial operations and/or to improve their reliability and lifetime. Technical fluids are often based on alkaline solutions with pH ranging from 9 to 12 [9–11] and this can be an issue for AAs, which normally exhibit high durability mainly in atmospheric environment. It is well known that, when exposed to atmospheric environment, AAs usually show a passive behavior due to the formation of a thin film of aluminum oxide (Al_2O_3) on the surface, which makes the corrosion rate (CR) negligible [12]. However, because of their amphoteric nature, AAs can exhibit corrosion when in contact with other media, such as alkaline or acidic solutions.

Some authors studied the electrochemical behavior of AAs in acidic environments investigating the performance of different corrosion inhibitors to slow down the dissolution [13–18]. Shahidi et al. investigated the kinetics of the corrosion process of AA 6061 tested in citric acid ($C_6H_8O_7$) as a function of temperature, pH, and the influence of Cl^- concentration. The authors found that the AA 6061 tested in $C_6H_8O_7$ at 25 °C exhibited an open circuit potential (E_{OCP}) of −0.518 V and a corrosion current density (i_{cor}) of 860 μA/cm^2. Furthermore, the same alloy tested in the presence of Cl^- showed an increase in corrosion damage. As a matter of fact, the electrochemical test carried out by adding 3.5 wt.% sodium chloride (NaCl) to the initial electrolyte highlights a decrease in the E_{OCP} to −0.621 V indicating a more negative potential and an increase in i_{cor} to 3500 μA/cm^2. Furthermore, this study highlights the strong influence of temperature and aggressiveness of the environment in the corrosion mechanisms [17].

Other studies report the corrosion behavior of AAs in alkaline media [19–28]. Yang et al. examined the surface morphology, microstructure, and corrosion mechanism of 3003 AA after alkaline etching in order to apply superhydrophobic treatments. It was found that the alkaline etching preferentially dissolves the Al matrix and the corrosion process forms $Al(OH)_3$ phases. At the same time, intermetallic phases (i.e., Al_6Mn) are preserved, inducing an increase in surface roughness and favoring the following hydrophobic surface modification [28]. Wang et al. carried out a study focusing on the corrosion behavior of AA 5052 to be applied as aluminum-air batteries. The anodes were tested in a NaOH 4 M solution dissolved in an ethylene glycol-water electrolyte. The electrochemical measurements performed on the AA 5052 immersed in the alkaline electrolyte revealed an open circuit potential of −1.56 V and a corrosion current density of 70,020 μA/cm^2. The results demonstrated that the addition of dicarboxylic acid to the alkaline electrolyte led to a decrease in the corrosion rate and a reduction in hydrogen production [24]. Eid et al. analyzed the behavior of AA 6063 in a solution of NaOH 0.1 M (pH = 13), aiming at reducing the kinetics of the corrosion process by adding different concentrations of methylcellulose in the electrolyte. They found an open circuit potential of −0.59 V and a corrosion current density (i_{cor}) of 376.8 μA/cm^2. The results show that, as the concentration of methylcellulose increases, a protective layer grows on the specimen surface, protecting the alloy from corrosion phenomena. The higher the concentration of methylcellulose in NaOH 0.1 M solution, the higher the inhibiting effect: a shift in the E_{OCP} towards more positive values and a reduction in the corrosion kinetics were measured. The electrochemical results recorded by adding 2000 ppm of methylcellulose to the initial electrolyte demonstrate a slightly more positive E_{OCP}, with an increased value of −0.55 V, and a significant decrease in i_{cor}, down to 160.7 μA/cm^2 [25].

Zaid et al. reported the corrosion behavior of AA 6061 in three different electrolytes, namely HCl 0.01 M, a slightly neutral solution of HCl 10^{-5} M, and NaOH 0.01 M alkaline solution, all containing 3.5 wt% NaCl, in order to determine the relationship between the corrosion morphology and the pH of the electrolyte [29]. The results showed that when AA 6061 is exposed to an acidic solution the E_{OCP} is found to be −0.74 V, with i_{cor} approximately equal to 10 μA/cm^2. The corrosion process results in a localized corrosion attack, specifically pitting corrosion, on the surface of the tested samples. Furthermore,

when AA 6061 is exposed to the alkaline solution, it exhibits the most negative E_{OCP} of −1.38 V and the highest corrosion current density, approximately 300 μA/cm^2. Conversely, this led to a general corrosion attack that exposed the underlying alloy microstructure.

The corrosion process for AA specimens tested in alkaline or acidic electrolytes revealed the microstructure of the alloys, highlighting the presence of secondary phases [30–40]. Various researchers have studied the electrochemical behavior of intermetallic compounds by measuring their E_{OCP} in different testing environments aiming at assessing their susceptibility to localized corrosion phenomena [31,32,37]. Depending on the chemical composition and the aggressiveness of the media, these secondary phases can act as anode or cathode in the corrosion mechanism, inducing different localized corrosion morphologies. In alkaline media, intermetallic compounds such as Mg_2Si behave like cathodic sites with respect to the surrounding AA matrix [30,36,38] inducing a micro-galvanic corrosion process, which leads to faster dissolution of the aluminum matrix at the interface with the intermetallic phase [30–38]. On the contrary, in acidic solutions these compounds behave like anodic sites, leading to pitting corrosion [33,41].

In order to improve the corrosion resistance performances of AAs, they are commonly subjected to surface anodization treatments. These surface modifications also can lead to enhanced tribological and mechanical properties, such as hardness and abrasion resistance [42]. Anodization treatment involves a controlled electrochemical process for the formation of micrometric oxide layers on the aluminum alloy surface. As the oxide layer forms porosities during its development, a sealing treatment is usually applied [43–45]. Traditionally, the sealing of the porous oxide layer was achieved through hydrothermal treatment in deionized or distilled boiling water baths [45]. Currently, various sealing solutions have been developed to enhance the corrosion resistance of the alloy and simultaneously achieve surfaces with new or optimized performances, such as hydrophobicity and ice resistance, thereby expanding their field of applications [28,46–49]. The corrosion resistance of anodized aluminum alloys in different environments has been extensively studied, including acidic and neutral solutions [50–54]. However, the behavior of anodized aluminum alloys in alkaline media is a topic that requires further investigation.

In this study, we aimed at investigating the influence of alkaline electrolyte parameters, i.e., pH and chloride addition, and anodizing treatment thicknesses on the corrosion behavior of different AAs currently used in mechanical industry. To achieve this, three different AAs (AA5083-H111, AA6082-T6, and AA7075-T6), provided in as-built conditions and with anodization treatments characterized by two thicknesses (10 and 40 μm), were tested in NaOH-based electrolytes at two different pH (pH = 12 and pH = 9) and the addition of Cl^- ions was also considered for the solution with pH = 9. For comparison's sake, the corrosion behavior of other metallic alloys commonly used in mechanical applications, i.e., carbon steel (C40), stainless-steel (AISI 304), and Cu-base alloys (Cu-Ni alloy and CW 617 N, respectively) were determined in the same alkaline environments. E_{OCP} measurements were carried out with the aim at building practical galvanic series in the investigated environments. In addition, anodic polarization curves were recorded to calculate the corrosion rate of the different investigated AAs. Lastly, the morphology and microstructure of the investigated AAs were examined after polarization measurements, using scanning electron microscopy (SEM).

The goal of this work is to make a contribution to the knowledge of corrosion behavior of aluminum alloys when used in specific applications where they can be in contact with alkaline solutions. Although some studies have already been carried out, different surface treatments can strongly influence the durability of the alloys.

Results show that the corrosion behavior of the three investigated alloys is influenced by (i) the aggressiveness of the testing environments; (ii) the thickness of the anodizing treatment; (iii) the alloy chemical composition; (iv) the distribution of intermetallic phases in the aluminum matrix.

2. Materials and Methods

2.1. Metallic Alloys

A selection of the AAs commonly applied in the field of industrial applications was considered in as-built conditions and after the anodization process. The three commercial AAs investigated are AA5083-H111, AA6082-T6, and AA7075-T6 (named AA 5, AA 6 and AA 7, respectively) and were sourced from AVIOMETAL, Varese, Italy. Their nominal compositions supplied in the technical data sheets are reported in Table 1. The AA5083-H111 alloy is a non-heat treatable medium-strength Al-Mg alloy. The H111 designation indicates that this alloy underwent a strain-hardening and partial annealing process for enhancing both strength and formability [4,55,56]. AA6082-T6 is an Al-Mg-Si alloy known for its favorable combination of strength, corrosion resistance, and weldability. AA7075-T6 is an Al-Zn alloy with a high strength-to-weight ratio suitable for lightweight applications. Both AA6082 and AA7075 underwent T6 treatment, which involves a two-step process consisting of a solution heat treatment followed by ageing. T6 treatment significantly improves the mechanical properties of the alloy, including strength, hardness, and resistance to deformation [4,55,57].

Table 1. Nominal composition of the investigated aluminum alloys (Al to balance).

	Si	Fe	Cu	Mn	Mg	Cr	Zn	Ti
AA 5 AB	0.40	0.40	0.10	0.40–1.00	4.00–4.90	0.05–0.25	0.25	0.15
AA 6 AB	0.70–1.30	<0.50	<0.10	0.40–1.00	0.60–1.20	<0.25	<0.2	<0.1
AA 7 AB	<0.40	<0.50	1.20–2.00	<0.3	2.10–2.90	0.18–0.28	5.10–6.10	<0.2

AA 5, AA 6, and AA 7 have been tested in their as-built condition (AB), and after two different anodization treatments leading to a nominal thickness of 10 µm (named I10), and 40 µm (hard anodization, named HA). Both treatments were industrially obtained by immersion in H_2SO_4 solution. The HA alloys were also tested after the sealing procedure (named S) by immersion of the samples in nickel acetate solution at room temperature.

For observing the microstructure of AA 5, AA 6, and AA 7, chemical etching was performed by dipping the samples in 40 mL of Keller's acid reagent for 20 s. The formulation used to prepare 200 mL of Keller's solution involves the use of 2 mL HF, 3 mL HCl, and 5 mL HNO_3 in 190 mL of H_2O as specified in the ASTM E407-07 standard [58]. After etching, samples were rinsed with distilled water and dried by a heat gun. Etched specimens were considered as reference for microstructural observations carried out by scanning electron microscope (SEM) (Philips XL20, Milan, Italy) and reported in Figure 1.

Comparing the three different alloys, secondary phases, well-known from the literature as intermetallic phases [32,34,37], can be observed: a larger amount is present in AA 5 AB and in AA 6 AB compared to AA 7 AB, where a limited amount is noted. Comparable morphology (round shape) and size distributions (<5 µm) are detected for all the intermetallic phases. From the EDS analysis reported in Figure 1, Mg_2Si intermetallic phase has been found in both AA 5 AB and AA 6 AB samples, while in the AA 7 AB alloy, Mg_2Si and Al_2Cu phases were detected. As reported in other studies [30,33,38,59], Mg_2Si is the typical intermetallic phase for AA 5083 and AA 6082.

For comparison purposes, medium carbon steel (C40) and austenitic stainless-steel (AISI 304) (both supplied by Lucefin Group, Brescia, Italy), two Cu-based alloys, such as an α, β′ brass CW617N (supplied by A.L.M.A.G. Azienda Lavorazioni Metallurgiche e Affini Gnutti, Brescia, Italy), and a Cu-Ni alloy commercially named FORMAPLAST 160 (supplied by RS acciai s.r.l., Florence, Italy) were also tested. Their nominal compositions from the technical data sheets are reported in Tables 2 and 3, respectively.

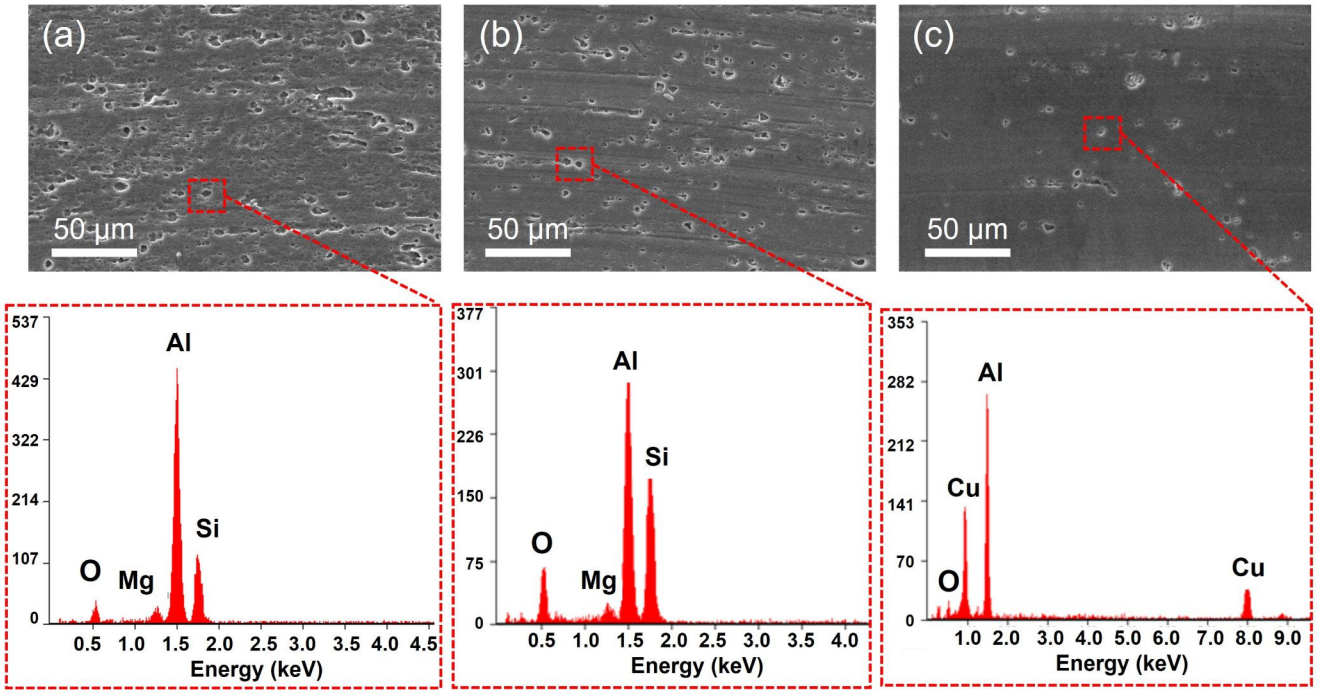


Figure 1. Metallographic observations of (**a**) AA 5 AB, (**b**) AA 6 AB, and (**c**) AA 7 AB. In the red box, intermetallic phases are highlighted and their EDS spectra are reported.

Table 2. Nominal composition of steels (C40 and AISI 304).

	C	Si	P	Mn	Cr	Mo	Ni	Fe
C 40	0.37–0.44	0.4	0.03	0.5–0.8	0.4	0.1	0.4	97.4–97.8
AISI 304	0.07	1.0	0.045	2.0	17.5–19.5	-	8.0–10.5	66.9–71.4

Table 3. Nominal composition of Cu-based alloys (CW 617N and Cu-Ni alloy).

	Sn	Fe	Zn	Pb	Ni	Si	Cu
CW 617 N	<0.3	<0.3	38.0–40.0	1.6–2.2	<0.1	<0.03	57.0–59.0
Cu-Ni alloy	-	-	-	-	1.50–2.50	-	88.9–91.5

2.2. Alkaline Solutions

Technical fluids commonly employed for operations in industrial plants are typically alkaline solutions with a pH ranging from 9 to 12 [9–11]. Moreover, some of these fluids, especially detergents, contain chloride ions (Cl^-) that can significantly compromise the corrosion resistance of the analyzed alloys. Therefore, to replicate these industrial conditions, three alkaline solutions were prepared. NaOH pellets (Sigma Aldrich, Milan, Italy (ACS reagent)) were added to demineralized water to obtain different concentrations: E1 solution has a concentration of 10^{-2} mol NaOH/L with a pH = 12, while E2 has a concentration of 10^{-5} mol NaOH/L and a pH equal to 9. In order to study the influence of Cl^- ions in the corrosion behavior of the selected alloys, E3 solution was prepared by adding 3.5 wt% NaCl (supplied by Sigma Aldrich, Milan, Italy) to E2 solution. The pH of the prepared electrolytes was checked using a CyberScan pH 310 pH meter (Fisher Scientific Italia, Segrate, MI, Italy) before and after each electrochemical measurement, in order to monitor any unexpected pH variation.

2.3. Characterization

All the alloys have been supplied as disks of 18 mm diameter and 4 mm thickness and a visual analysis was performed with the aim of detecting the surface texture. All the AA disks showed circular concentric crests over the surface due to a chip removal process. The presence of signs with non-uniform directions due to an abrasion process were observed on the carbon and stainless-steel surfaces. The supplied specimens were used for electrochemical and microstructural characterization after degreasing their surfaces with acetone.

Electrochemical tests were carried out by using a conventional electrochemical cell adopting two different configurations: a two-electrode configuration was applied to measure E_{OCP} and a three-electrode setup to record anodic polarization curves. For measuring E_{OCP}, the sample was mounted in a Teflon sample holder acting as a working electrode (WE) and connected to a potentiostat (Amel, model 7050, Milan, Italy) together with a saturated calomel electrode (SCE) working as reference electrode (RE). To record anodic polarization curves (E-log(i) plots), a platinum wire was added to act as the counter electrode (CE). Each electrochemical measurement was carried out using a temperature-controlled electrochemical cell set at 30 °C. E_{OCP} values were recorded after 2 h of sample immersion in E1, E2, and E3 solutions and the reported values are the average of three measurements.

Anodic polarization curves were recorded starting from 0.1 V lower than E_{OCP} up to 1.0 V higher than E_{OCP}, applying a scan rate of 0.167 mV/s. The surface area of each sample exposed to the electrolyte was 2.010 ± 0.007 cm^2. To ensure reproducibility of results, all measurements were repeated at least three times. From E-log(i) plots, the determination of corrosion current density values (i_{cor}) was carried out by applying the Tafel extrapolation method in the range of $\pm$25 mV with respect to the E_{OCP} values. Then, the corrosion rates (CRs) were calculated according to ASTM-G102-89 [60], using Equation (1):

$$CR = K_1 \times (i_{cor}/\rho) \times EW \text{ [mm/yr]} \quad (1)$$

where EW is the equivalent weight of the sample [g] and $K_1 = 3.27 \times 10^{-3}$ [mm·g/μA·cm·yr] is a constant reported in [60] to obtain CR in mm/yr.

Lastly, to support the electrochemical results, microstructural analyses were carried out after anodic polarization tests by using a scanning electron microscope (SEM) Philips XL20, Milan, Italy.

3. Results and Discussion

The electrochemical assessment of all the investigated alloys is reported and discussed starting with the E_{OCP} values measured in E1, E2, and E3 alkaline electrolytes. These data, representing the tendency of the alloys to oxidize when in contact with an electrolyte, have been treated to build galvanic series for each of the considered media. In Figure 2, the trend of E_{OCP} versus time of AA 6 AB in all the tested solutions is reported as typical example, while for brevity's sake E_{OCP} values after 2 h of immersion in E1, E2, and E3 are collectively reported as histogram plots in Figures 3 and 4, respectively.

Regarding AAs, E_{OCP} measurements revealed that these alloys in AB condition exhibit the most negative values. In particular, the AA 6 AB sample both in E1 and E2 (-1.48 ± 0.04 $V_{(SCE)}$ and -1.06 ± 0.04 $V_{(SCE)}$, respectively) and AA 5 AB tested in E3 (-1.02 ± 0.04 $V_{(SCE)}$) are the most active alloys in the correspondent galvanic series. Among the three aluminum alloys, AA 7 AB samples always show less negative E_{OCP} values. Furthermore, AA alloys with I10 treatment exhibit similar values to the AB condition when tested in E1, while E_{OCP} shift towards less negative values when tested in E2 and E3 (both with pH = 9). Also in this case, AA 7 I10 samples show less negative E_{OCP} values within the I10 samples. All HA-treated samples (both in sealed and non-sealed conditions) show comparable potential values in the range between $-0.5 \div -0.7$ $V_{(SCE)}$ in all the tested media and less negative E_{OCP} values, especially in E1. Comparing potential values of the investigated aluminum alloys in E2 and E3 (same

pH, but addition of 3.5 wt% NaCl in E3), a general shift towards more negative values is observed in E3, except for the A 6 and A 7 in AB condition that strangely showed slightly higher E_{OCP} values.

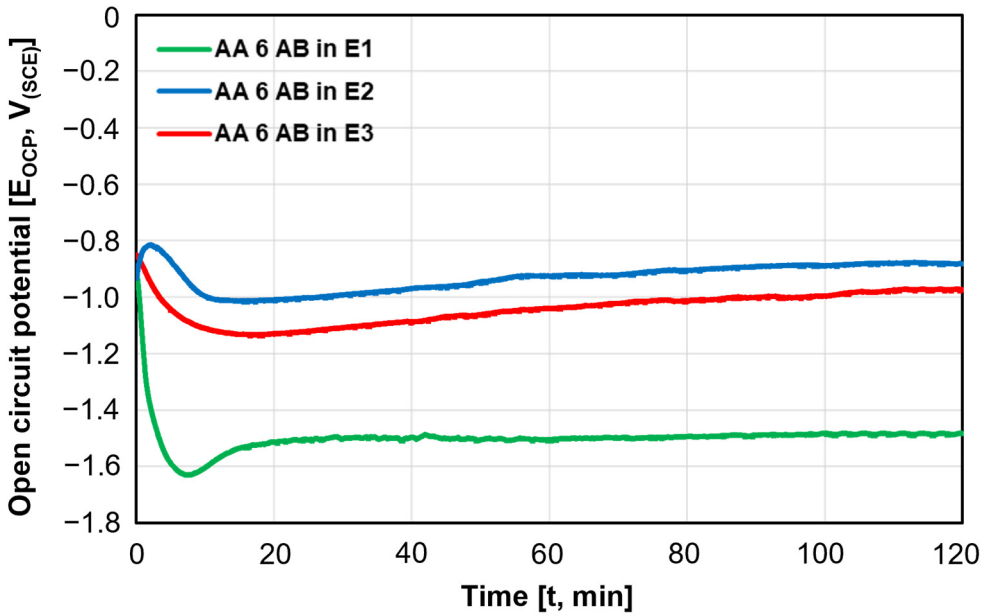


Figure 2. Evolution of E_{OCP} measured for AA 6 AB for 2 h in E1, E2, and E3 media.

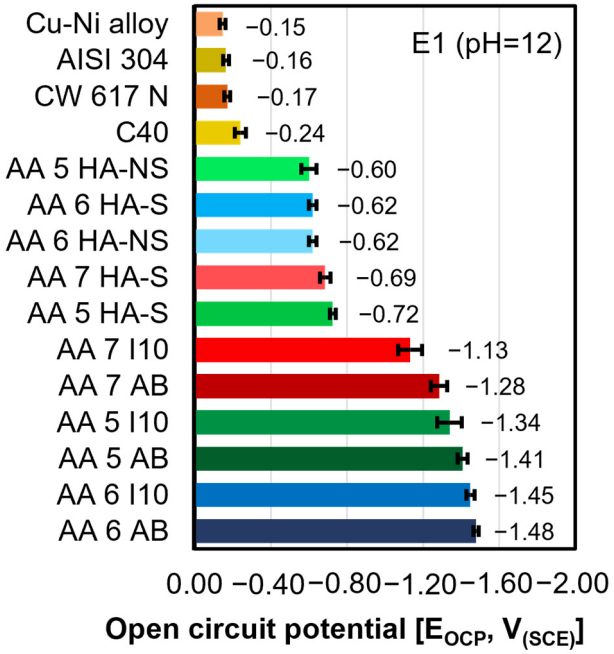


Figure 3. Galvanic series built from the E_{OCP} values for all the investigated alloys tested in the E1 solution.

All the reported results indicate that among the tested samples in the AB condition, AA 7 exhibits the lowest oxidation tendency by showing less negative E_{OCP} values in all the environments taken into account. In addition, a comparison of E_{OCP} values measured for the I10 samples in E1 and E2 solutions highlights that an increase in the solution alkalinity (pH = 12 for E1 and pH = 9 for E2) leads to more negative potential values. I10 treatment promotes the shifting of the potential toward less negative values, but only when in contact with less alkaline solutions (i.e., E2 and E3), probably due to the small thickness of the anodization treatment (nominally 10 μm). On the contrary, HA treatment (anodization

thickness of 40 µm) tested in E1 solution was shown to be less prone to oxidation than I10. HA treatment induces a relevant increase in the potential values in all the investigated solutions, thanks to the increased thickness of the surface treatment.

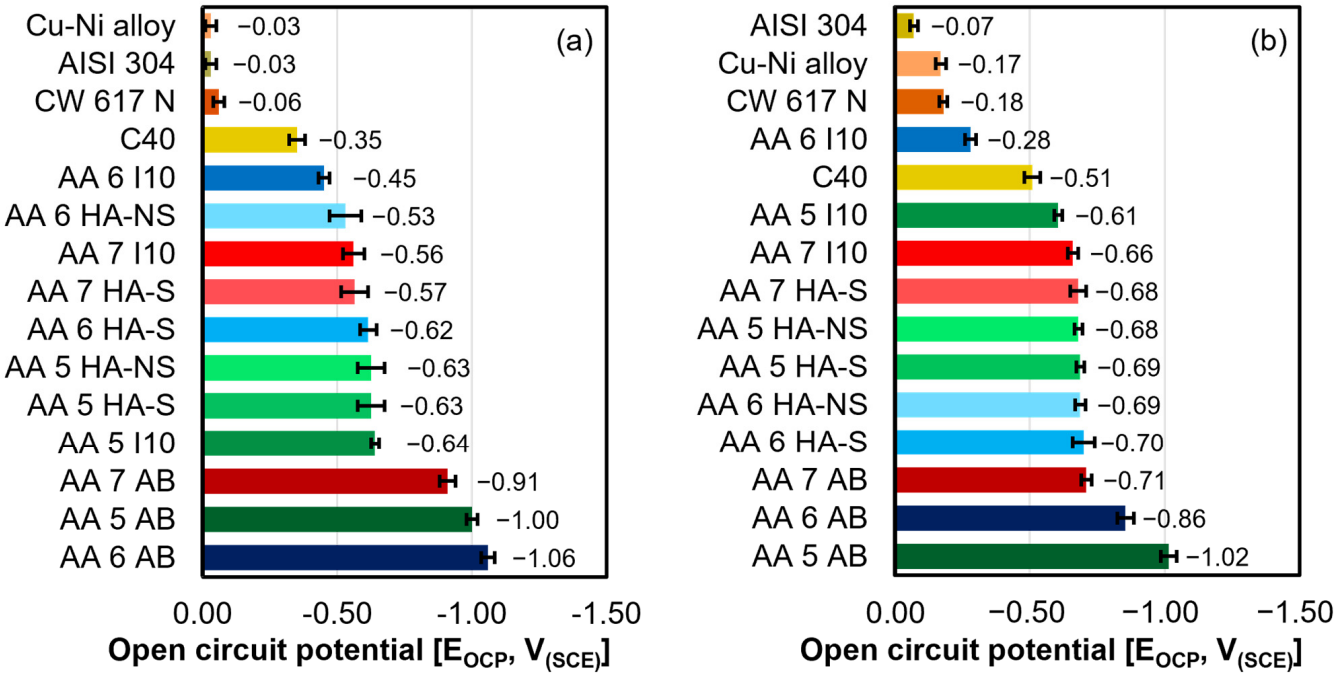


Figure 4. Galvanic series built from the E_{OCP} values for all the investigated alloys tested in (**a**) E2 and (**b**) E3 solutions.

All the other tested alloys, such as Cu-based alloys (CW 617 N and Cu-Ni alloy), carbon steel (C40), and stainless-steel (AISI 304), show less negative E_{OCP} values than all the aluminum alloys in E1, E2, and E3. Indeed, the less negative E_{OCP} values are found for Cu-Ni alloy in E1 (-0.15 ± 0.04 $V_{(SCE)}$) and E2 (-0.03 ± 0.04 $V_{(SCE)}$) and for AISI 304 in E3 (-0.07 ± 0.04 $V_{(SCE)}$) [61–64]. Comparing the three galvanic series, it is possible to observe that the carbon steel (C40) specimen tested in E2 exhibited more negative values compared to the ones in E1 solution. This behavior can be attributed to the favorable formation of magnetite, a stable iron oxide film (Fe_3O_4) that occurs on the carbon steel surface when exposed to alkaline environments with pH > 10 [65,66]. In E2 and E3 (pH = 9), the formation of magnetite is shown to be less favorable compared to E1 and the presence of Cl^- ions further decreases E_{OCP} values (E_{OCP} @E3 < E_{OCP} @E2 < E_{OCP} @E1).

The scientific literature provides a limited amount of data regarding the electrochemical behavior of AAs in an alkaline environment. Only few data related to AA 5052 and AA 6061 (recorded in the same temperature conditions of our study, but with alkaline environments with different NaOH concentration) have been found and reported in Table 4. The experimental data of Figures 3 and 4 are in line with the ones found in the literature: AA5052 exhibits more negative E_{OCP} values compared to the ones recorded in E1 for AA 5 AB due to the fact that it was tested in a more concentrated NaOH solution compared to E1. Furthermore, AA 6 AB in E1 exhibited $E_{OCP} = -1.48$ $V_{(SCE)}$ which is comparable with the value reported for AA 6061 in NaOH solutions with concentrations ranging from 0.05 M to 0.5 M (Table 4).

As E_{OCP} measurements only describe the thermodynamic behavior, anodic polarization curves (E-log(i) plot) were recorded to obtain information about corrosion rate. Figures 5 and 6 report the anodic polarization curves of the aluminum alloys in AB condition in E1, E2, and E3 and with I10 treatment in E1, respectively.

Table 4. E_{OCP}, i_{cor}, CR in different alkaline media derived from literature data.

Alloys	Electrolyte	E_{OCP} [$V_{(SCE)}$]	i_{cor} [μA/cm^2]	CR [μm/yr]	Ref.
AA 5052	4 M NaOH in $C_2H_6O_2$	−1.56	70,000	767,522	[24]
AA 5052	4 M NaOH	−1.54	70,020	767,742	[27]
AA 6061	0.05 M NaOH	−1.48	676	7410	[19]
	0.1 M NaOH	−1.48	1750	13,750	
	0.25 M NaOH	−1.49	2340	25,690	
	0.5 M NaOH	−1.50	5570	65,150	
AA 6063	0.05 M NaOH	−1.55	404	4400	[67]
	0.25 M NaOH	−1.57	2090	22,780	
	0.5 M NaOH	−1.59	3260	35,530	

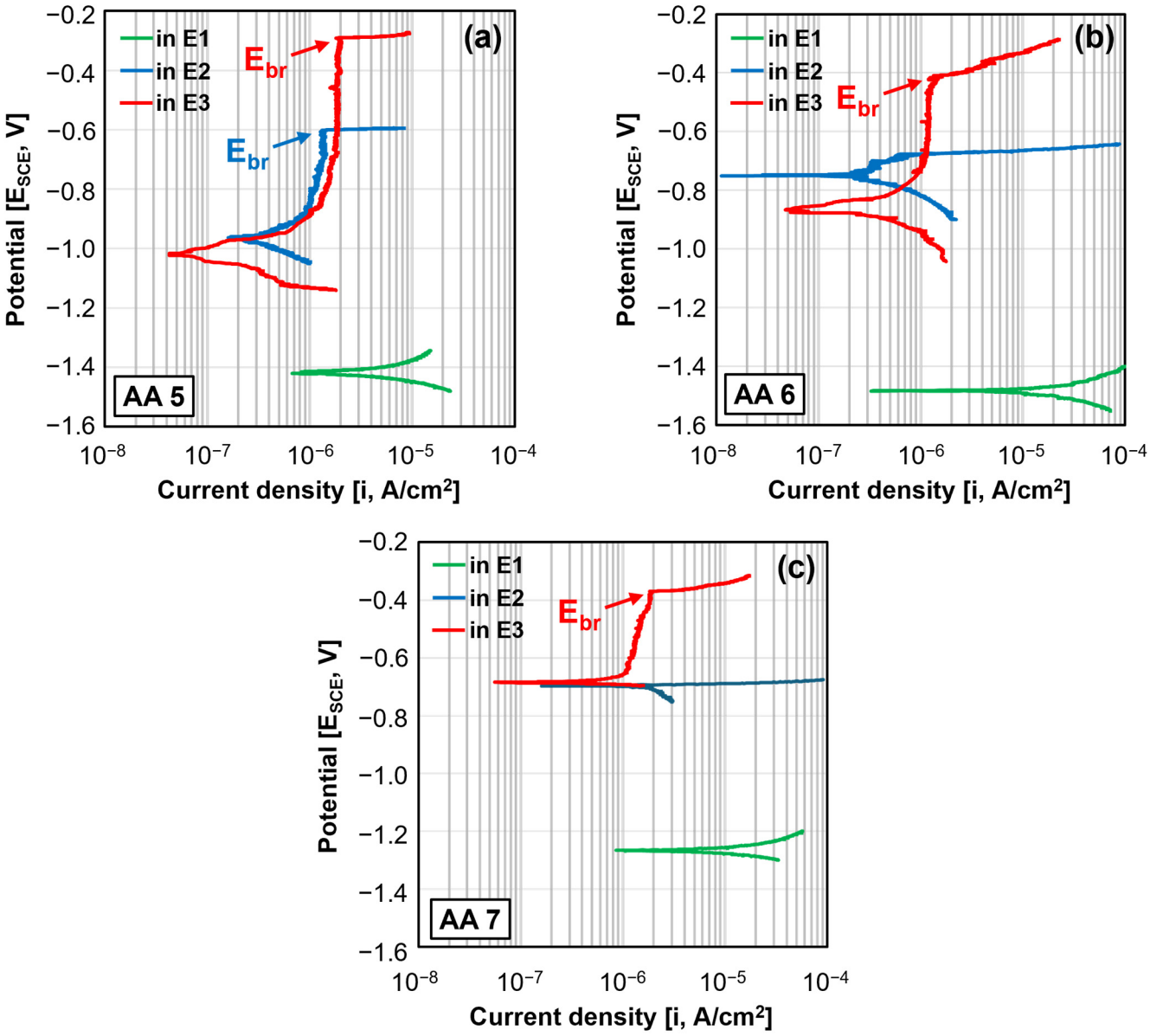


Figure 5. Anodic polarization curves in E1, E2, and E3 electrolytes of aluminum alloys in AB condition: (**a**) AA 5 AB, (**b**) AA 6 AB, and (**c**) AA 7 AB.

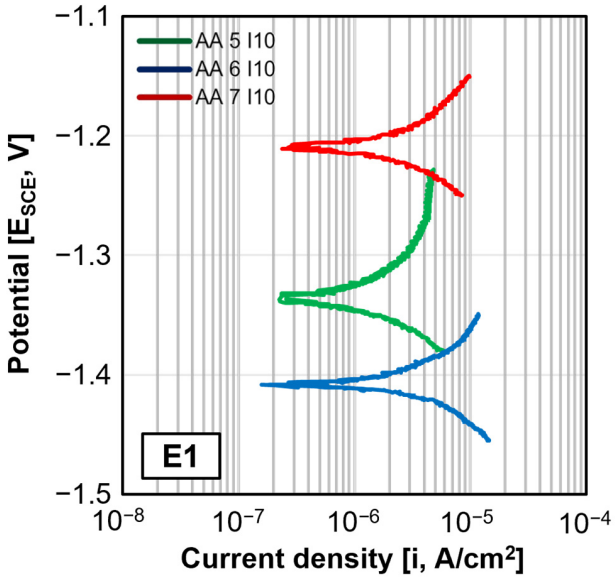


Figure 6. Anodic polarization curves of I10-treated aluminum alloys samples in E1 solution.

In E1 (green line), the polarization curves of all the three aluminum alloys in AB condition (Figure 5) reveal an increasing trend of current density as a function of the electrical potential, which represents an active behavior. In terms of E_{OCP} values, these curves are in the most negative region of the E-log(i) plots, consistently with the previously discussed E_{OCP} results. Among the AB samples, AA 6 exhibits the highest current density values, indicating a significant increase in the kinetic of the corrosion process (and consequently the highest corrosion rate value has been determined). Furthermore, the curves of the three aluminum alloys in AB condition in E1 display the highest current density values (shift in the right part of the plot) when compared to those obtained for the same alloys in E2 (red line) and in E3 (blue line). In E2, it is possible to observe that all the three AAs show a passive behavior, highlighting a potential increase where the current density is almost constant. Similar breakdown potential (E_{br}) values have been detected: $E_{br} = -0.30\ V_{(SCE)}$ for AA 5 AB, $E_{br} = -0.40\ V_{(SCE)}$ for AA 6 AB, and $E_{br} = -0.36\ V_{(SCE)}$. However, the polarization curve corresponding to AA 5 AB exhibits a more extensive passivation zone compared to the others, due to the most negative E_{OCP} values. Remarkably, all the three curves exhibit similar current density ranges, ranging from 0.3–0.7 $\mu A/cm^2$.

The addition of Cl^- (E3 solution) induces a shift toward higher current density values for all the three AAs compared to E2. In addition, only AA 5 AB samples shows a clear passive zone even if a reduction in the breakdown potential was recorded ($E_{br} = -0.60\ V_{(SCE)}$), while AA 6 and 7 exhibited an active behavior.

The kinetic behavior of the corrosion process for the aluminum alloys treated both with I10 and HA was investigated through anodic polarization tests. HA (both in S and NS conditions) in all the investigated environments and I10 samples tested in E2 and E3 exhibited very low passivation current density (order of magnitude: $10^{-9}\ A/cm^2$), thus indicating that the anodization treatment is very effective. The E-log(i) characteristic curves recorded for I10 in E1-treated samples are reported in Figure 6. These curves show the anodic and cathodic branches indicating that I10 samples in E1 solution behave like active alloys. Comparing these anodic polarization curves with the ones obtained for samples in AB condition, it is possible to observe that the latter is shifted towards lower i_{cor} values, indicating that HA treatment leads to a reduction in the kinetic of the corrosion process.

To quantify the kinetic of the corrosion process, the Tafel extrapolation method was applied on E-log(i) curves to determine i_{cor} and CR parameters (Table 5) for AB and I10 conditions tested in E1. In E2 and E3 solutions, a significant instrumental noise did not allow Tafel extrapolation. On the three different AA samples in AB condition in E1, the

highest CR value has been found for AA 6 AB, while AA 7 AB exhibits the lowest one. In general, lower values of CR for I10-treated samples have been observed than those determined for samples in AB condition.

Table 5. Characteristic values of anodic polarization curves of AB and I10-treated aluminum alloys recorded in E1. i_{cor} values were calculated by Tafel graphical extrapolation.

Sample	i_{cor} [μA/cm^2]	CR [μm/yr]
AA 5 AB	4.03 ± 0.04	45.0 ± 0.4
AA 6 AB	8.05 ± 0.07	87.6 ± 0.8
AA 7 AB	3.71 ± 0.03	41.4 ± 0.4
AA 5 I10	2.87 ± 0.03	32.1 ± 0.4
AA 6 I10	1.99 ± 0.02	21.7 ± 0.2
AA 7 I10	0.93 ± 0.04	10.4 ± 0.4

Other researchers studied the electrochemical behavior of AA 5, AA 6, and AA 7 in NaOH solutions by using the E-log(i) characteristic curves [19,29,67]. The most representative data from the literature are reported in Table 4. Higher i_{cor} and CR values are reported in the literature compared to the ones obtained in this study, mainly related to the fact that solutions with higher NaOH concentration have been used in the reported literature.

Microstructural analysis was performed on the surface of AA 5, AA 6, and AA 7 in the AB, I10, and HA conditions, after the electrochemical measurements, to obtain qualitative information about the morphology of the corrosion attack.

Microstructural observation of AA 5, AA 6, and AA 7 in AB condition tested in E1, E2, and E3 electrolytes are reported in Figure 7. A uniform corrosion attack was evident due to an increase in surface roughness. It is also observed how a variation in the aggressiveness of the solution (i.e., increase in pH) can affect the surface response due to the corrosion attack. The higher the pH, the stronger the corrosion damage and the more evident the dissolution of aluminum. Moreover, especially for AA 6, evidence of localized corrosion attack is depicted in correspondence with the boundary region between the intermetallic phase (previously described in Figure 1) and the aluminum matrix, forming grooves around the intermetallic particle [30]. This was observed mainly on the surface of the AA 6 AB sample because of the high concentration of intermetallic phases dispersed in the matrix. The same alloys tested in the E2 did not exhibit any significant corrosion damage, while samples tested in E3 reveal evidence of a slight corrosion attack due to the addition of Cl^- in the electrolyte (Figure 7). Overall, morphological analysis confirms that the corrosion process occurring on the sample in AB conditions immersed in E1 is more severe than that occurring in E2 and E3 solutions.

Morphological and microstructural investigations carried out on 10 μm-anodized samples (AA 5 I10, AA 6 I10, AA 7 I10) after electrochemical characterization in E1, E2, and E3 electrolytes are shown in Figure 8.

Morphological observations performed after electrochemical characterization of aluminum alloys AA 5, AA 6, and AA 7 in I10 condition in E1 mainly reveal cracks of the anodizing treatment, while surface cracks are less visible for the samples exposed to E2 and E3 solutions, especially for AA 5 and AA 6. Moreover, it is also possible to observe a homogenous distribution of micro-pores mainly due to surface treatment defects. Such defects can explain the corrosion performances of AA 5, AA 6, and AA 7 in I10 condition previously discussed.

Finally, morphological investigations of aluminum alloys AA 5, AA 6, and AA 7 in HA condition, both sealed and unsealed, exposed to E1, E2, E3 solutions are reported in Figures 9 and 10. These micrographs do not show significant corrosion damage except those for samples AA 5 HA (in sealed and unsealed conditions, tested in E1) which show cracks and discontinuities in the protective layer. The comparison of morphological observations for aluminum alloys AA 5, AA 6, and AA 7 in the I10 and HA-S conditions highlights

that the thickness of the anodization treatment is very important and confirms the data obtained by electrochemical characterizations.

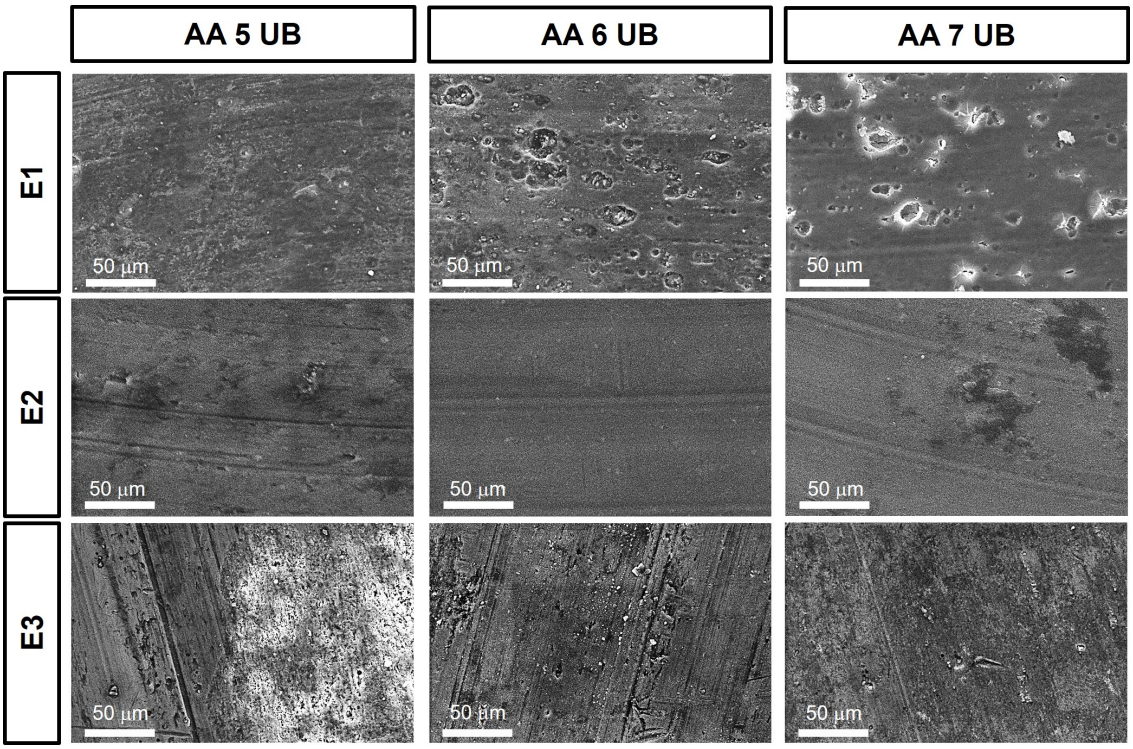


Figure 7. SEM micrographs of aluminum alloys AA 5, AA 6, and AA 7 in AB condition after anodic polarization tests performed in E1, E2, and E3.

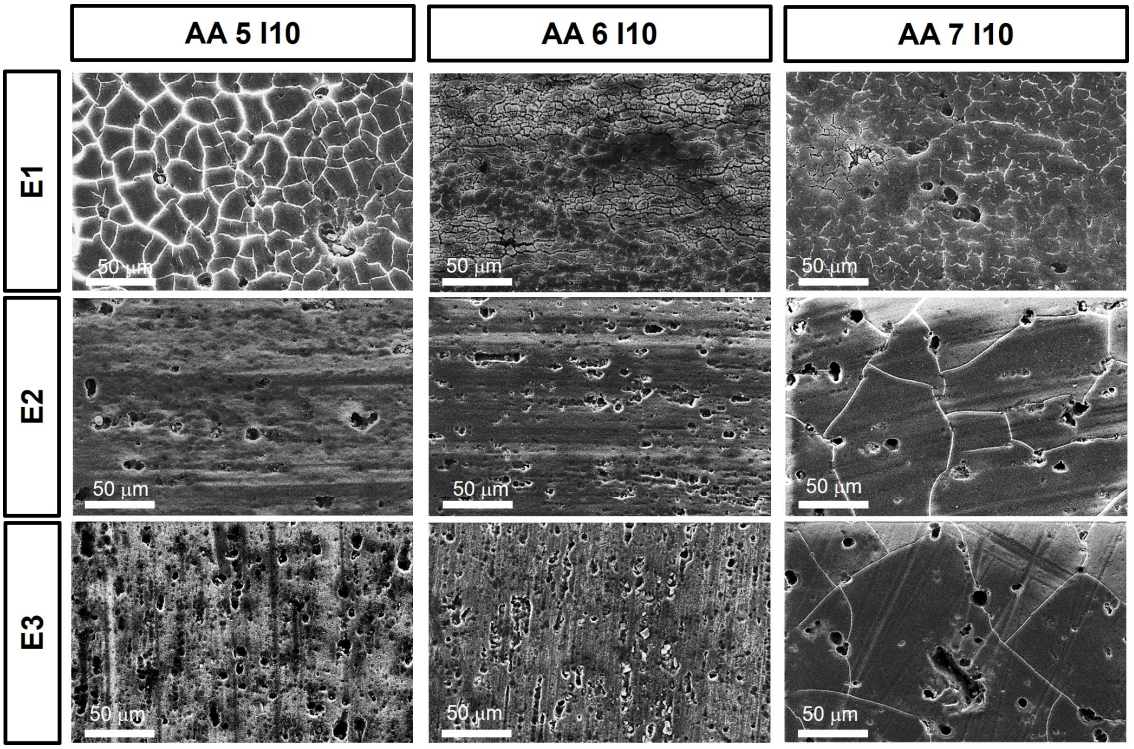


Figure 8. SEM micrographs of aluminum alloys AA 5, AA 6, and AA 7 in I10 condition after anodic polarization tests performed in E1, E2 and E3.

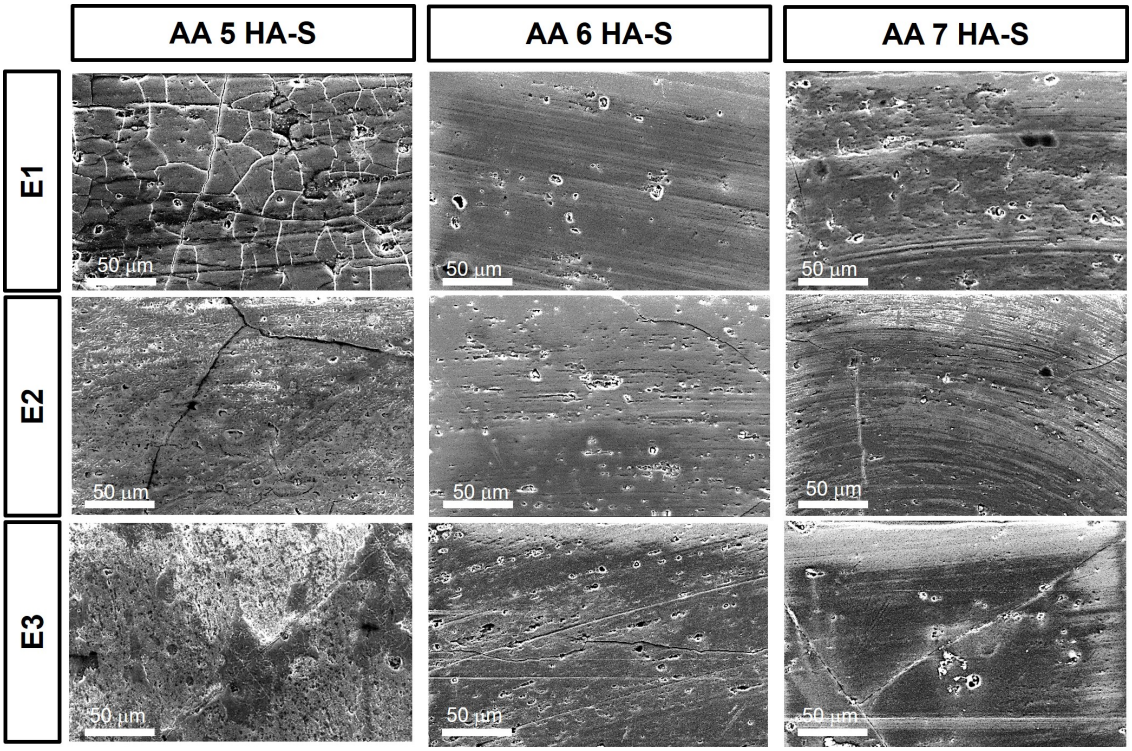


Figure 9. SEM micrographs of aluminum alloys AA 5, AA 6, AA 7 in HA-S condition after anodic polarization tests in E1, E2, and E3.

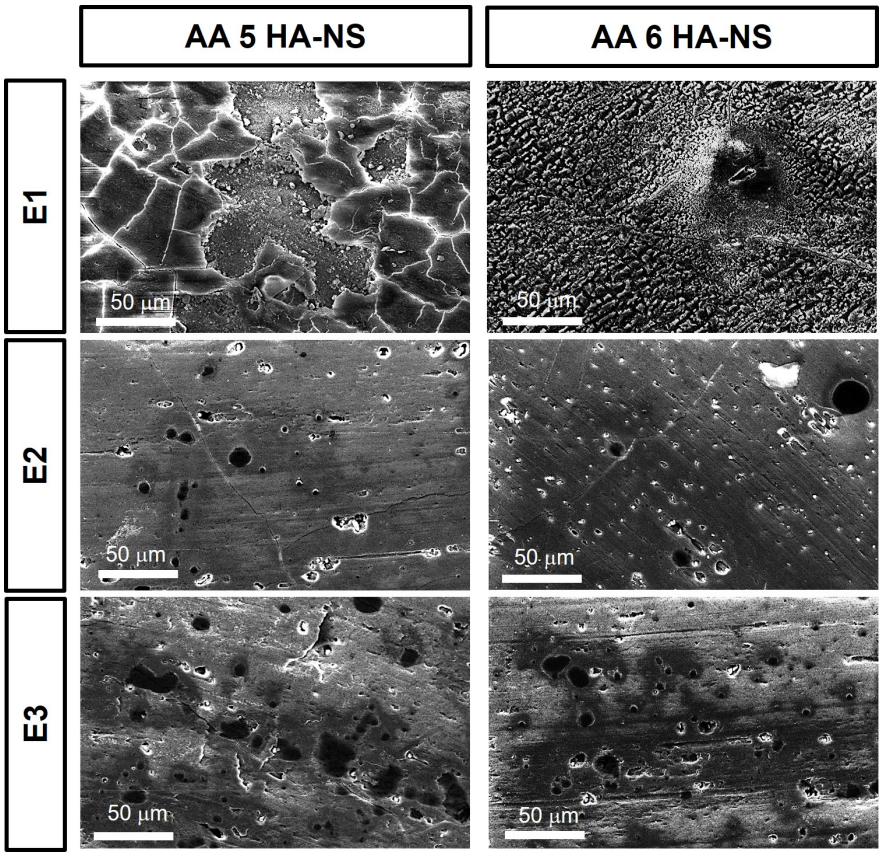


Figure 10. SEM micrographs of aluminum alloys in HA-NS condition after anodic polarization tests in E1, E2, and E3.

4. Conclusions

The corrosion behavior of three different aluminum alloys in as-built (AB) and anodized conditions (I10, HA-S, HA-NS) was investigated in alkaline electrolytes by electrochemical techniques and microstructural observations.

The principal outcomes of the study are reported as follows:

a. The as-built samples were found to be the most electronegative ones, holding the lowest positions in the galvanic series. Among the samples, AA 6 AB, tested in E1 and E2 electrolytes, as well as AA 5 AB, tested in E3, exhibited the most electronegative E_{OCP} values. Conversely, AA 7 AB appeared to be the most electropositive in all the considered environments;
b. The E_{OCP} values measured for the three alloys in I10 condition increased with the aggressiveness of the testing solution, whereas the HA-S and HA-NS samples exhibited no significant variation in E_{OCP} values across any of the environments considered;
c. Comparing the E-log(i) characteristic curves obtained for the three alloys in AB condition in E1 with those recorded in E2 and E3 solutions reveals a variation in their electrochemical behavior. In the former electrolyte, specimens show an active behavior, while in E2 and E3 an active-passive behavior was observed. All the anodized samples in E2 and E3 exhibited the lowest current density and consequently the lowest corrosion rate;
d. The electrochemical behavior of AA samples analyzed in all the considered electrolytes was found to be dependent on the pH of the environment as well as the thickness of the anodization treatment.

Lastly, further studies will be carried out to investigate the electrochemical behavior of the same aluminum alloys, with also other surface treatments, in acidic solutions. The evaluation of their thermodynamic and kinetic behavior as functions of different environmental characteristics and materials features will allow a complete picture of aluminum alloys in different conditions occurring in industrial plants.

Author Contributions: Conceptualization, G.M. and M.C.B.; methodology, R.F. and G.M.; software, R.F.; validation, R.F., G.M. and M.C.B.; formal analysis, R.F. and G.M.; investigation, R.F.; resources, M.C.B.; data curation, R.F.; writing—original draft preparation, R.F.; writing—review and editing, G.M. and M.C.B.; visualization, R.F.; supervision, G.M. and M.C.B.; project administration, M.C.B.; funding acquisition, M.C.B. All authors have read and agreed to the published version of the manuscript.

Funding: This research received no external funding.

Institutional Review Board Statement: Not applicable.

Informed Consent Statement: Not applicable.

Data Availability Statement: The data presented in this study are available on request from the corresponding author. The data are not publicly available due to confidentiality reasons.

Conflicts of Interest: The authors declare no conflicts of interest.

References

1. Watari, T.; Nansai, K.; Nakajima, K. Major metals demand, supply, and environmental impacts to 2100: A critical review. *Resour. Conserv. Recycl.* **2021**, *164*, 105107. [CrossRef]
2. Liu, G.; Müller, D.B. Addressing sustainability in the aluminum industry: A critical review of life cycle assessments. *J. Clean. Prod.* **2012**, *35*, 108–117. [CrossRef]
3. Brough, D.; Jouhara, H. The aluminium industry: A review on state-of-the-art technologies, environmental impacts and possibilities for waste heat recovery. *Int. J. Thermofluids* **2020**, *1–2*, 100007. [CrossRef]
4. Davis, J.R. Physical Metallurgy of Aluminum Alloys. In *Metals Handbook Desk Edition*; ASM International: Detroit, MI, USA, 2018; pp. 437–442.
5. Totten, G.; MacKenzie, D.S. *Handbook of Aluminum: Physical Metallurgy and Processes*, 1st ed.; Marcel Dekker, Inc.: New York, NY, USA, 2003; Volume 1, ISBN 0824704940.

6. Qbau, N.; Nam, N.; Hien, N.; Ca, N. Development of light weight high strength aluminum alloy for selective laser melting. *J. Mater. Res. Technol.* **2020**, *9*, 14075–14081. [CrossRef]
7. Hossain, N.; Chowdhury, M.A.; Iqbal, A.P.; Ahmed, A.F.; Islam, S. Corrosion behavior of aluminum alloy in NaOH and Syzygium Samarangense solution for environmental sustainability. *Curr. Res. Green Sustain. Chem.* **2022**, *5*, 100254. [CrossRef]
8. Mogucheva, A.; Babich, E.; Kaibyshev, R. Microstructure and Mechanical Properties of An Al-Mg-Sc-Zr Alloy Subjected to Extensive Cold Rolling. In Proceedings of the 13th International Conference on Aluminum Alloys (ICAA13), Pittsburgh, PA, USA, 3–7 June 2012; pp. 1773–1778.
9. Brinksmeier, E.; Meyer, D.; Huesmann-Cordes, A.; Herrmann, C. Metalworking fluids—Mechanisms and performance. *CIRP Ann. Manuf. Technol.* **2015**, *64*, 605–628. [CrossRef]
10. El Sachat, A.; Meristoudi, A.; Markos, C.; Sakellariou, A.; Papadopoulos, A.; Katsikas, S.; Riziotis, C. Characterization of Industrial Coolant Fluids and Continuous Ageing Monitoring by Wireless Node—Enabled Fiber Optic Sensors. *Sensors* **2017**, *17*, 568. [CrossRef]
11. Bird, R.W. Aqueous alkaline cleaners: A better alternative. *Met. Finish.* **1995**, *93*, 10–20. [CrossRef]
12. Quadri, T.W.; Akpan, E.D.; Olasunkanmi, L.O.; Fayemi, O.E.; Ebenso, E.E. Fundamentals of Corrosion Chemistry. In *Environmentally Sustainable Corrosion Inhibitors: Fundamentals and Industrial Applications*; Elsevier: Amsterdam, The Netherlands, 2021; pp. 25–45, ISBN 9780323854054.
13. Kisasoz, A. Corrosion behavior of alloy AA6063-T4 in HCl and NaOH solutions. *Mater. Test.* **2018**, *60*, 478–482. [CrossRef]
14. Reboul, M.C.; Baroux, B. Metallurgical aspects of corrosion resistance of aluminium alloys. *Mater. Corros.* **2011**, *62*, 215–233. [CrossRef]
15. Adams, F.V.; Akinwamide, S.O.; Obadele, B.; Olubambi, P.A. Comparison study on the corrosion behavior of aluminum alloys in different acidic media. *Mater. Today Proc.* **2021**, *38*, 1040–1043. [CrossRef]
16. Pruthviraj, R.D.; Rashmi, M. Electrochemical Studies of Aluminium 7075 Alloy in Different Concentration of Acid Chloride Medium. *J. Mater. Sci. Eng.* **2016**, *5*, 221. [CrossRef]
17. Shahidi, M.; Gholamhosseinzadeh, M. Electrochemical evaluation of AA6061 aluminum alloy corrosion in citric acid solution without and with chloride ions. *J. Electroanal. Chem.* **2015**, *757*, 8–17. [CrossRef]
18. Kruger, J. Passivity. In *Corrosion: Fundamentals, Testing, and Protection*; ASM International: Detroit, MI, USA, 2003; Volume 13A, pp. 61–67.
19. Kumari, P.R.; Nayak, J.; Shetty, A.N. Corrosion behavior of 6061/Al-15 vol. pct. SiC(p) composite and the base alloy in sodium hydroxide solution. *Arab. J. Chem.* **2016**, *9*, S1144–S1154. [CrossRef]
20. Kharitonov, D.S.; Dobryden, I.; Sefer, B.; Ryl, J.; Wrzesińska, A.; Makarova, I.V.; Bobowska, I.; Kurilo, I.I.; Claesson, P.M. Surface and corrosion properties of AA6063-T5 aluminum alloy in molybdate-containing sodium chloride solutions. *Corros. Sci.* **2020**, *171*, 108658. [CrossRef]
21. Huang, Y.-S.; Shih, T.-S.; Wu, C.-E. Electrochemical behavior of anodized AA6063-T6 alloys affected by matrix structures. *Appl. Surf. Sci.* **2013**, *264*, 410–418. [CrossRef]
22. Joshi, S.; Fahrenholtz, W.G.; O'keefe, M.J. Electrochemical Characterization of Al 7075-T6 Surface Oxide after Alkaline Treatments. *J. Electrochem. Soc.* **2011**, *158*, C296–C301. [CrossRef]
23. Andreatta, F.; Lohrengel, M.; Terryn, H.; de Wit, J. Electrochemical characterisation of aluminium AA7075-T6 and solution heat treated AA7075 using a micro-capillary cell. *Electrochimica Acta* **2003**, *48*, 3239–3247. [CrossRef]
24. Wang, D.; Zhang, D.; Lee, K.; Gao, L. Performance of AA5052 alloy anode in alkaline ethylene glycol electrolyte with dicarboxylic acids additives for aluminium-air batteries. *J. Power Sources* **2015**, *297*, 464–471. [CrossRef]
25. Eid, S.; Abdallah, M.; Kamar, E.; El-Etre, A.Y. Corrosion Inhibition of Aluminum and Aluminum Silicon Alloys in Sodium Hydroxide Solutions by Methyl Cellulose. *J. Mater. Environ. Sci.* **2015**, *11*, 892–901.
26. Xhanari, K.; Finšgar, M. Organic corrosion inhibitors for aluminum and its alloys in chloride and alkaline solutions: A review. *Arab. J. Chem.* **2019**, *12*, 4646–4663. [CrossRef]
27. Wang, D.; Li, H.; Liu, J.; Zhang, D.; Gao, L.; Tong, L. Evaluation of AA5052 alloy anode in alkaline electrolyte with organic rare-earth complex additives for aluminium-air batteries. *J. Power Sources* **2015**, *293*, 484–491. [CrossRef]
28. Yang, H.; Gao, Y.; Qin, W.; Sun, J.; Huang, Z.; Li, Y.; Li, B.; Sun, J. A robust superhydrophobic surface on AA3003 aluminum alloy with intermetallic phases in-situ pinning effect for corrosion protection. *J. Alloys Compd.* **2022**, *898*, 163038. [CrossRef]
29. Zaid, B.; Saidi, D.; Benzaid, A.; Hadji, S. Effects of pH and chloride concentration on pitting corrosion of AA6061 aluminum alloy. *Corros. Sci.* **2008**, *50*, 1841–1847. [CrossRef]
30. Jin, Z.; Cai, C.; Hashimoto, T.; Yuan, Y.; Kang, D.; Hunter, J.; Zhou, X. Alkaline etching and desmutting of aluminium alloy: The behaviour of Mg_2Si particles. *J. Alloys Compd.* **2020**, *842*, 155834. [CrossRef]
31. Eckermann, F.; Suter, T.; Uggowitzer, P.J.; Afseth, A.; Schmutz, P. The influence of MgSi particle reactivity and dissolution processes on corrosion in Al–Mg–Si alloys. *Electrochim. Acta* **2008**, *54*, 844–855. [CrossRef]
32. Buchheit, R.G. A Compilation of Corrosion Potentials Reported for Intermetallic Phases in Aluminum Alloys. *J. Electrochem. Soc.* **1995**, *142*, 3994. [CrossRef]
33. Gupta, R.K.; Sukiman, N.L.; Fleming, K.M.; Gibson, M.A.; Birbilis, N. Electrochemical Behavior and Localized Corrosion Associated with Mg2Si Particles in Al and Mg Alloys. *ECS Electrochem. Lett.* **2012**, *1*, C1–C3. [CrossRef]
34. Rana, R.S.; Purohit, R.; Das, S. Reviews on the Influences of Alloying Elements on the Microstructure and Mechanical Properties of Aluminum Alloys and Aluminum Alloy Composites. *Int. J. Sci. Res. Publ.* **2012**, *2*, 1–7.

35. Birbilis, N.; Buchheit, R.G. Investigation and Discussion of Characteristics for Intermetallic Phases Common to Aluminum Alloys as a Function of Solution pH. *J. Electrochem. Soc.* **2008**, *155*, C117. [CrossRef]
36. de Miera, M.S.; Curioni, M.; Skeldon, P.; Thompson, G. The behaviour of second phase particles during anodizing of aluminium alloys. *Corros. Sci.* **2010**, *52*, 2489–2497. [CrossRef]
37. Birbilis, N.; Buchheit, R.G. Electrochemical Characteristics of Intermetallic Phases in Aluminum Alloys. *J. Electrochem. Soc.* **2005**, *152*, B140–B151. [CrossRef]
38. Linardi, E.; Haddad, R.; Lanzani, L. Stability Analysis of the Mg_2Si Phase in AA 6061 Aluminum Alloy. *Procedia Mater. Sci.* **2012**, *1*, 550–557. [CrossRef]
39. Andreatta, F.; Terryn, H.; de Wit, J. Effect of solution heat treatment on galvanic coupling between intermetallics and matrix in AA7075-T6. *Corros. Sci.* **2003**, *45*, 1733–1746. [CrossRef]
40. De Wit, J.H.W. Local Potential Measurements with the SKPFM on Aluminium Alloys. *Electrochim. Acta* **2004**, *49*, 2841–2850. [CrossRef]
41. Li, L.L.; Zhang, B.; Tian, B.; Zhou, Y.; Wang, J.Q.; Han, E.H.; Ke, W. SVET Study of Galvanic Corrosion of Al/Mg_2Si Couple in Aqueous Solutions at Different pH. *J. Electrochem. Soc.* **2017**, *164*, C240–C249. [CrossRef]
42. Martínez-Viademonte, M.P.; Abrahami, S.T.; Hack, T.; Burchardt, M.; Terryn, H. A Review on Anodizing of Aerospace Aluminum Alloys for Corrosion Protection. *Coatings* **2020**, *10*, 1106. [CrossRef]
43. Tsangaraki-Kaplanoglou, I.; Theohari, S.; Dimogerontakis, T.; Wang, Y.-M.; Kuo, H.-H.; Kia, S. Effect of alloy types on the anodizing process of aluminum. *Surf. Coatings Technol.* **2006**, *200*, 2634–2641. [CrossRef]
44. Shahzad, M.; Chaussumier, M.; Chieragatti, R.; Mabru, C.; Rezai-Aria, F. Influence of anodizing process on fatigue life of machined aluminium alloy. *Procedia Eng.* **2010**, *2*, 1015–1024. [CrossRef]
45. Ofoegbu, S.U.; Fernandes, F.A.; Pereira, A.B. The Sealing Step in Aluminum Anodizing: A Focus on Sustainable Strategies for Enhancing Both Energy Efficiency and Corrosion Resistance. *Coatings* **2020**, *10*, 226. [CrossRef]
46. Egorkin, V.S.; Mashtalyar, D.V.; Gnedenkov, A.S.; Filonina, V.S.; Vyaliy, I.E.; Nadaraia, K.V.; Imshinetskiy, I.M.; Belov, E.A.; Izotov, N.V.; Sinebryukhov, S.L.; et al. Icephobic Performance of Combined Fluorine-Containing Composite Layers on Al-Mg-Mn–Si Alloy Surface. *Polymers* **2021**, *13*, 3827. [CrossRef] [PubMed]
47. Liu, S.; Chen, J.; Zhang, D.; Wang, Y.; He, Z.; Guo, P. Properties of Micro-Arc Oxidation Coatings on 5052 Al Alloy Sealed by SiO_2 Nanoparticles. *Coatings* **2022**, *12*, 373. [CrossRef]
48. Mashtalyar, D.V.; Nadaraia, K.V.; Belov, E.A.; Imshinetskiy, I.M.; Sinebrukhov, S.L.; Gnedenkov, S.V. Features of Composite Layers Created Using an Aqueous Suspension of a Fluoropolymer. *Polymers* **2022**, *14*, 4667. [CrossRef] [PubMed]
49. Kaseem, M.; Dikici, B.; Dafali, A.; Fattah-Alhosseini, A. Self-assembly of coumarin molecules on plasma electrolyzed layer for optimizing the electrochemical performance of AZ31 Mg alloy. *J. Magnes. Alloys* **2023**, *11*, 1618–1628. [CrossRef]
50. Gu, J.; Zhang, X.; Yu, L. Investigation on Anodized 5052 Aluminum Alloy and its Corrosion Resistance in Simulated Acid Rain. *Int. J. Electrochem. Sci.* **2023**, *18*, 100336. [CrossRef]
51. Yu, X.; Zhang, G.; Zhang, Z.; Wang, Y. Research on corrosion resistance of anodized and sealed 6061 aluminum alloy in 3.5% sodium chloride solution. *Int. J. Electrochem. Sci.* **2023**, *18*, 100092. [CrossRef]
52. Usman, B.J.; Scenini, F.; Curioni, M. Corrosion Testing of Anodized Aerospace Alloys: Comparison Between Immersion and Salt Spray Testing using Electrochemical Impedance Spectroscopy. *J. Electrochem. Soc.* **2020**, *167*, 041505. [CrossRef]
53. Zhang, Y.; Chen, Y.; Bian, G.; Zhang, Y. Electrochemical behavior and corrosion mechanism of anodized 7B04 aluminum alloy in acid NaCl environments. *J. Alloys Compd.* **2021**, *886*, 161231. [CrossRef]
54. Thompson, G.E.; Zhang, L.; Smith, C.J.E.; Skeldon, P. Boric/Sulfuric Acid Anodizing of Aluminum Alloys 2024 and 7075: Film Growth and Corrosion Resistance. *Corrosion* **1999**, *55*, 1052–1061. [CrossRef]
55. Emmanuel, A.; Fayomi, O.; Akande, I. Aluminium Alloys as Advanced Materials: A short communication. *IOP Conf. Ser. Mater. Sci. Eng.* **2021**, *1107*, 012024. [CrossRef]
56. Huang, C.; Wu, Z.; Huang, R.; Wang, W.; Li, L. Mechanical Properties of AA5083 in Different Tempers at Low Temperatures. *IOP Conf. Ser. Mater. Sci. Eng.* **2017**, *279*, 012002. [CrossRef]
57. MacKenzie, D.S. Metallurgy of Heat Treatable Aluminum Alloys. In *Aluminum Science and Technology*; ASM International: Detroit, MI, USA, 2018; pp. 411–437.
58. *ASTM E407−23*; Standard Practice for Microetching Metals and Alloys. ASTM International: West Conshohocken, PA, USA, 2023.
59. Yasakau, K.A.; Zheludkevich, M.L.; Lamaka, S.V.; Ferreira, M.G.S. Role of intermetallic phases in localized corrosion of AA5083. *Electrochim. Acta* **2007**, *52*, 7651–7659. [CrossRef]
60. *ASTM G102*; Standard Practice for Calculation of Corrosion Rates and Related Information from Electrochemical Measurements. ASTM International: West Conshohocken, PA, USA, 2023.
61. Berne, C.; Andrieu, E.; Reby, J.; Sobrino, J.-M.; Blanc, C. The Electrochemical Behavior of α,β′-Brass in Basic $NaNO_3$ Solutions. *J. Electrochem. Soc.* **2015**, *162*, C648–C656. [CrossRef]
62. Assouli, B.; Srhiri, A.; Idrissi, H. Characterization and control of selective corrosion of α,β′-brass by acoustic emission. *NDT E Int.* **2003**, *36*, 117–126. [CrossRef]
63. Berne, C.; Andrieu, E.; Reby, J.; Sobrino, J.-M.; Blanc, C. Dissolution Kinetics of α,β′-Brass in Basic $NaNO_3$ Solutions. *J. Electrochem. Soc.* **2016**, *163*, C7–C15. [CrossRef]

64. Freire, L.; Carmezim, M.; Ferreira, M.; Montemor, M. The passive behaviour of AISI 316 in alkaline media and the effect of pH: A combined electrochemical and analytical study. *Electrochim. Acta* **2010**, *55*, 6174–6181. [CrossRef]
65. Song, G.D.; Jeon, S.-H.; Son, Y.-H.; Kim, J.G.; Hur, D.H. Galvanic effect of magnetite on the corrosion behavior of carbon steel in deaerated alkaline solutions under flowing conditions. *Corros. Sci.* **2018**, *131*, 71–80. [CrossRef]
66. Zheng, H.; Dai, J.-G.; Li, W.; Poon, C.S. Influence of chloride ion on depassivation of passive film on galvanized steel bars in concrete pore solution. *Constr. Build. Mater.* **2018**, *166*, 572–580. [CrossRef]
67. Deepa, P.; Padmalatha, R. Corrosion behaviour of 6063 aluminium alloy in acidic and in alkaline media. *Arab. J. Chem.* **2017**, *10*, S2234–S2244. [CrossRef]

Disclaimer/Publisher's Note: The statements, opinions and data contained in all publications are solely those of the individual author(s) and contributor(s) and not of MDPI and/or the editor(s). MDPI and/or the editor(s) disclaim responsibility for any injury to people or property resulting from any ideas, methods, instructions or products referred to in the content.